TITAN'S MAGNETOSPHERIC INTERACTION

FRITZ M. NEUBAUER
Universität zu Köln

DONALD A. GURNETT
University of Iowa

JACK D. SCUDDER and RICHARD E. HARTLE
Goddard Space Flight Center

Voyager 1 encountered Titan on 12 Nov. 1980 around 0540:20 spacecraft event time when Titan was located in Saturn's outer magnetosphere. In this chapter we review the plasma, magnetic field and plasma wave observations and analyses from the plasma dynamist's point of view. In particular we discuss the following: (1) The incident Saturn magnetoplasma was characterized by Alfvénic and sonic Mach numbers 1.9 and 0.57, respectively, and a fast magnetohydrodynamic Mach number of 0.55; (2) The incident plasma was found to interact with the atmosphere of Titan rather than an internal magnetic field leading to the formation of an induced magnetosphere by mass pickup and associated field-line draping in a similar way to that of Venus; (3) In the tail of the induced magnetosphere a central region characterized by a strong reduction of $\geq$ *700 eV electrons and substantial mass loading due to the addition of* N^+ *or* N_2^+/H_2CN^+ *associated with strong field-line draping could be distinguished from the surrounding regions of* H^+ *mass loading and relatively weak magnetic field-line draping; (4) In the central, strong draping region a four-lobe magnetotail has been identified where the lobes can either be north or south of the neutral sheet of the tail and be due to draping over either the dayside or nightside hemisphere of Titan; (5) An upper limit of* 7×10^{20} *Gauss* cm^3 *has been derived for an internal rotationally aligned magnetic dipole moment; (6) A loss rate of* 10^{24} N^+ *or* N_2^+/H_2CN^+ *ions per second has been estimated from observations of the tail.*

Titan, as every planet or satellite in the solar system, will be found to be ultimately enclosed by a streaming magnetized plasma if an observer were to move outward from its center through its interior and subsequently through its extensive atmosphere (chapter by Hunten et al.). In this chapter the interaction of Titan with the incident plasma flow is discussed. It is especially interesting for various reasons. In the first place, this interaction determines an important part of the mass balance of the atmosphere. In addition to the losses and gains of atmospheric species through the surface (e.g. by condensation and evaporation etc.) and the gain of mass by incoming particulate matter, the mass balance of the atmosphere is determined by losses (and sometimes perhaps gains). Losses due to the electrodynamic interaction of the satellite with its plasma environment, as well as classical Jeans escape of neutrals. The losses at the same time represent a gain for the surrounding plasma. If Titan is located in Saturn's magnetosphere, it will contribute to the plasma population of the magnetosphere (see chapter by Schardt et al.).

Another interesting consideration is Titan's magnetospheric interaction as a special case of a fundamental problem in space plasma physics, i.e. the interaction between a magnetized plasma flow and a planet or satellite. The detailed physics of this interaction depends on the properties of the incident flow and the characteristics of the body. Several cases have been studied in the past: the case of a planet without an appreciable atmosphere but with a substantial global magnetic field in the case of Mercury; the case of a planet with an atmosphere but without a substantial magnetic field like that of Venus; the case of a planet with an atmosphere and a magnetic field like Earth's; and the case of neither an atmosphere nor a global magnetic field like that of the Earth's moon, to mention only a few.

It has been known for almost four decades that Titan possesses a substantial atmosphere (Kuiper 1944). The Voyager mission has now given us a detailed picture of this atmosphere (see chapter by Hunten et al.; *Science* 10 Apr. 1981; Smith et al. 1982; Strobel and Shemansky 1982; Lindal et al. 1983). The question is then whether the incident plasma interacts directly with Titan's atmosphere or whether the atmosphere is, so to speak, protected by a substantial internal magnetic field diverting the plasma flow, before it reaches the atmosphere. For favorable conditions in Titan's interior constrained by general cosmochemical considerations and the observed bulk density and size of the satellite, one can derive a global magnetic field of 100 nT at Titan's equator (Neubauer 1978). One of the objectives of the close encounter of Voyager 1 with Titan was to investigate for the first time the detailed nature of Titan's interaction with the surrounding plasma flow and to answer the question of the existence of an internal field. Our present observational knowledge of Titan's interaction is based almost exclusively on the data from the single encounter of Voyager 1. However, Titan's orbital radius of 20.2 Saturn radii (R_S) is such that the satellite may be located in the solar wind, in the magnetosheath of Saturn, or in Saturn's magnetosphere depending on the dy-

namic state of the magnetosphere and Titan's orbital phase (Acuna and Ness 1980). It therefore experiences widely varying plasma conditions in the incident flow (Wolf and Neubauer 1982). Nevertheless, many significant results of general validity have been derived from the Voyager 1 encounter.

Our review of the electrodynamic interaction between Titan and Saturn's magnetosphere based on Voyager 1 encounter data and general physical principles will begin with a brief description of Voyager 1 experiment characteristics necessary for the synthesis of the observations (Sec. I). This is followed by a summary of the encounter characteristics (Secs. II and III). We shall then consider the possibility of an internal magnetic field (Sec. IV). The extensive discussion of Titan's induced magnetosphere (Sec. V) will constitute the main body of the chapter.

I. EXPERIMENT DESCRIPTIONS

Several experiments contributed to the observations defining the plasma flow associated with Titan. *In situ* measurements were performed by the magnetometer, plasma science, plasma wave, planetary radio astronomy and low-energy charged particles experiment onboard Voyager 1. The ultraviolet spectrometer experiment also contributed to the overall picture. Results have been published in special journal issues of *Science* (10 Apr. 1981) and *Journal of Geophysical Research* (1 Mar. 1982). We shall emphasize here the use of the magnetic field, plasma and plasma wave data. For detailed descriptions of the experiments we refer the reader to a special issue of *Space Science Reviews* (Nov. Dec. 1977).

During Titan encounter the magnetometer experiment was operating at its highest sampling rate, one vector measurement every 0.060 s and its highest sensitivity, 8.8 nT full scale, $\pm$ 0.0022 nT quantization step size. The accuracy is estimated to be $\pm$ 0.05 nT.

The Voyager plasma instrument consisted of four potential modulated Faraday cups: three (A, B, C) arranged as a triad equally disposed about an axis pointing in the earthward (nearly solar) direction, supplemented by a single cup (D) whose cone of sensitivity had its axis almost perpendicular to that of the triad. The D-cup axis pointed towards the direction of cororational flow in Saturn's magnetosphere for the inbound part of the Saturn encounter trajectory. All four cups made both high- and low-energy resolution measurements of the ion velocity distribution functions; the D-cup measured ion and electron distribution functions alternately. The energy per charge range for both electrons and ions extended from 10 eV to 5950 eV with contiguous energy converage. It was broken into two intervals from 10 to 140 eV (E_1-mode) and 140 to 5950 eV (E_2-mode) for electrons. A complete measurement cycle with electron and low energy resolution ion measurements (L-mode) was carried out every 96 s, and for high energy resolution ions every (M-mode) 2 $\times$ 96 s. The E_1-, E_2- or L-mode in order E_1, L, E_2 were completed in 3.84 s each

with 2θ.2 s between two consecutive measuring intervals. Note the substantial gaps in time coverage particularly for the electrons. The M-mode was not used for the Titan work.

The plasma wave experiment used the two orthogonal 10-m electric antennas also used by the planetary radio astronomy experiment. A 16-channel spectrum analyzer with four channels per decade from 10 Hz to 56.2 Hz provided the necessary frequency resolution. One scan through all channels was performed every 4 s.

II. ENCOUNTER GEOMETRY

The Titan encounter occurred on 12 November 1980 at a minimum flyby distance of 6969 km from Titan's center at Saturn local time 1330. Closest approach occurred at 0540:20 spacecraft event time (SCET) in UT and the crossing of the orbital plane at Titan at 0543:07 SCET. The fact that the orbital plane crossing of Titan occurred very near closest approach turned out to be very useful for our investigations.

The flyby trajectory relative to Titan is shown projected on the XY-plane in Fig. 1. The axes of our coordinate system X, Y, Z with its origin at the center of Titan point towards the direction of ideal corotational flow, away from Saturn and perpendicular to the orbital plane, respectively. The flyby velocity was 17.3 km s^{-1}. Because of the 8°.7 tilt of the trajectory with respect to the orbital plane, the velocity components in the XY-plane and along the $(-Z)$ direction were 17.1 and 2.6 km s^{-1}, respectively. The flyby data therefore cover only a few minutes. Figure 1 also shows two ideal wake regions under the assumption of a flyby in the magnetosphere with ideal corotational flow and flyby in an ideal solar wind with flow radially from the Sun. The terminator is also shown for Titan. Since the encounter occurred a few months after Saturn's equinox, the northern pole of Titan was sunlit.

III. PROPERTIES OF INCIDENT PLASMA FLOW DURING TITAN ENCOUNTER

Because the encounter occurred close to local noon an interesting question was where Titan would be found: in the magnetosphere, in the magnetosheath or even in the solar wind. It turned out, that Titan was well within the outer magnetosphere of Saturn with Saturn's magnetopause crossings observed 5 times between 22.8 and 23.7 R_S (Ness et al. 1981; Bridge et al. 1981*a*; Gurnett et al. 1981*a*). The magnetic field data displayed in Fig. 2 indicate a magnetic field of magnitude $B = 5$ nT and a direction perpendicular to the XY-plane in the region surrounding Titan's plasma wake. Table I gives a summary of magnetic field and plasma properties considered to be most representative of the incident flow conditions. They have been derived from ob-

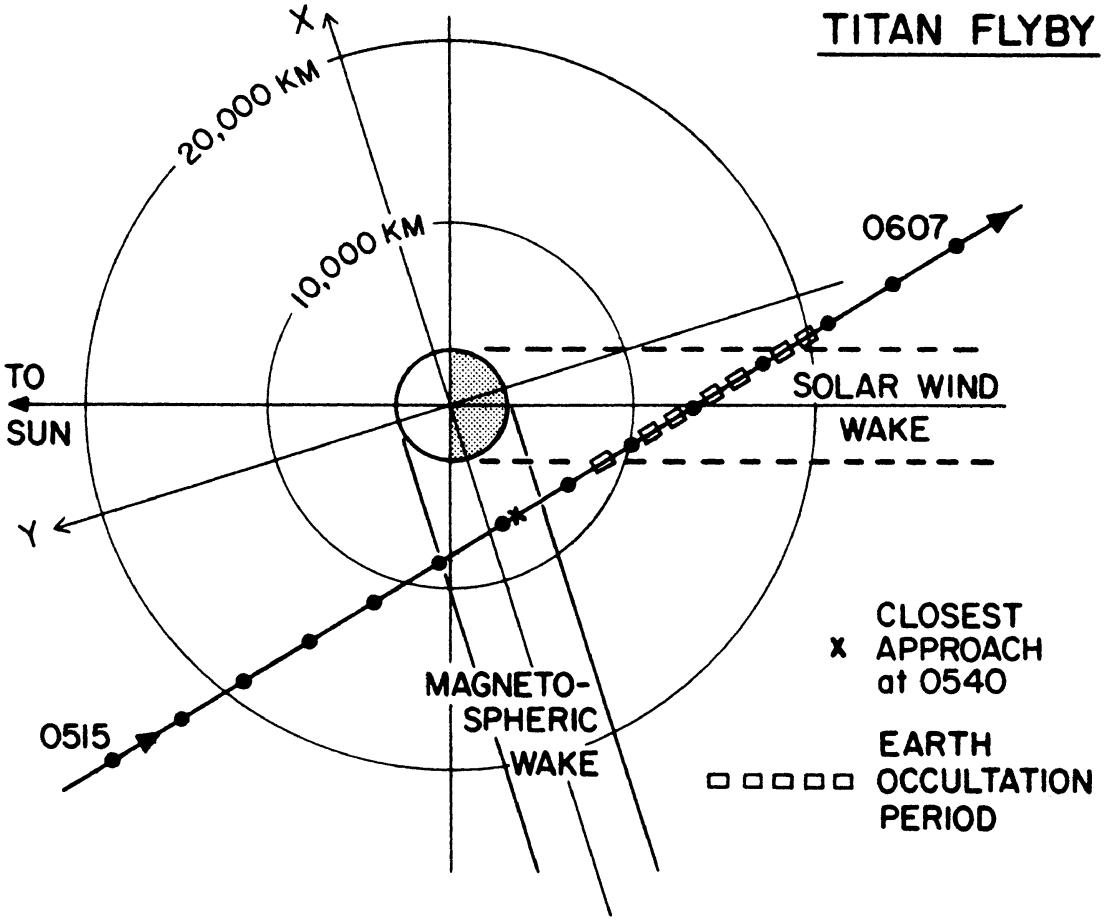

Fig. 1. Voyager trajectory past Titan projected into Saturn's equatorial plane with hypothetical magnetospheric and solar wind wake regions also indicated (from Ness et al. 1982*b*). The coordinate axes *X* and *Y* are also shown.

servations just outside the interaction region. For example, the ion results constitute a synthesis of the data points marked by one and eight shown in Fig. 6 in Sec. V.A. The velocities should be compared with the velocity of ideal corotational flow at Titan's orbit, i.e. 200 km s^{-1}. The ion and electron measurements (Hartle et al. 1982) yield densities which are consistent with the plasma wave electron densities (Gurnett et al. 1982*b*). The variability is considered small enough for our following discussions.

Although the ion fractions and temperatures may still change to some extent after further analysis, the general picture which Table I provides is not expected to change. We note that the pressure is dominated by the plasma pressure in the incident flow. The two characteristic speeds in plasma flow problems, i.e. the Alfvén speed V_A and the speed of sound V_S are such that the respective Mach numbers are 1.9 and 0.57. Choosing the lower-limit electron density $n_e = 0.1$ cm^{-3} and no N^+-ions $M_A \approx 0.5$. The expression for the sonic speed corresponds to the result of collisionless theory for perpendicular propagation. It is interesting to note that the combination of Mach numbers derived above has not been encountered before in any study of the interaction between a planet or satellite and its magnetoplasma environment.

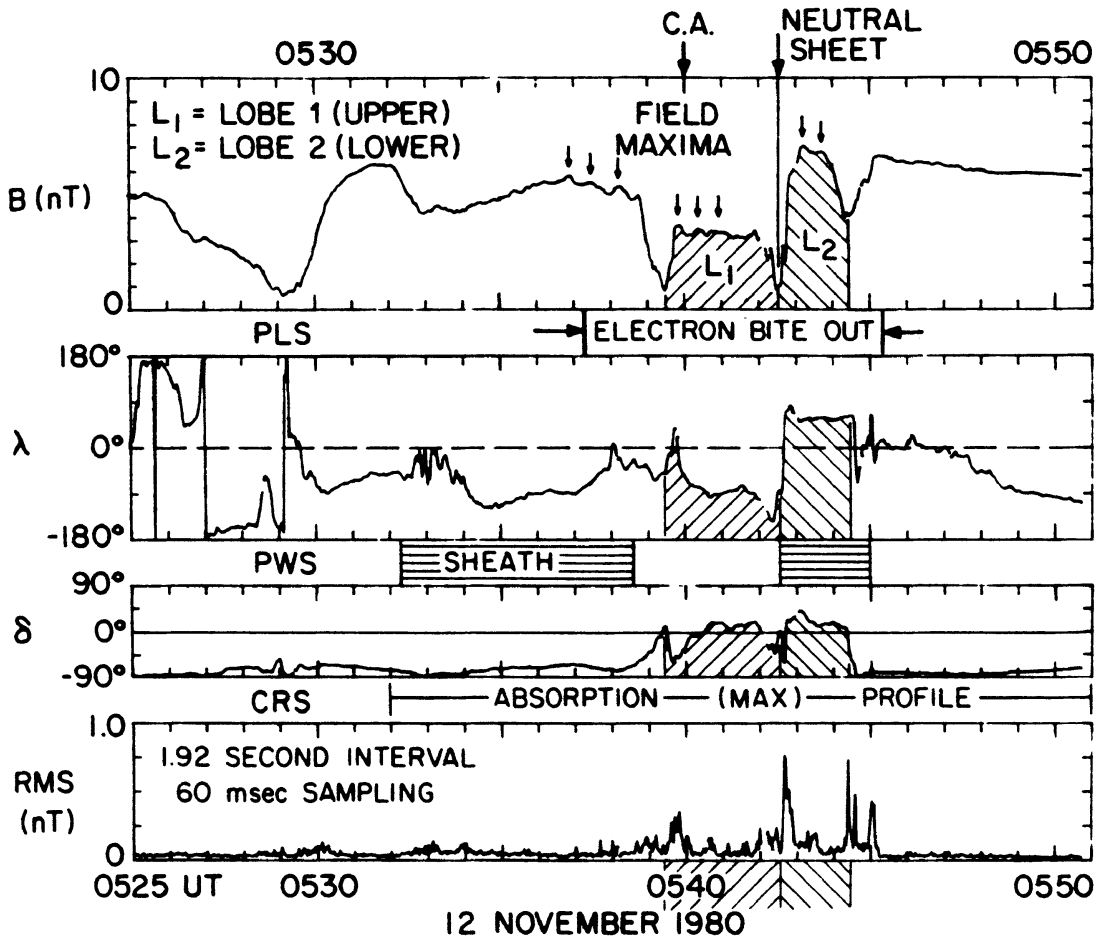

Fig. 2. Magnetic field observations in Saturn longitude system (SLS) coordinates during Titan close approach (C.A.). B, λ and δ are magnitude, longitude and elevation, respectively. For definition of SLS coordinates see Desch and Kaiser (1981*a*). The values plotted are 1.92 s averages. Also shown are the Pythagorean mean rms values. Significant intervals in the plasma science (PLS), plasma wave (PWS) and cosmic ray experiment (CRS) observations are also indicated (from Ness et al. 1982*b*).

Whether a fast magnetohydrodynamic (MHD) bow shock is formed depends on the fast Mach number which turned out to be 0.55. Hence no bow shock is expected. An independent test of this result will be presented in Sec. IV. The flow can nominally be characterized by superalfvénic, subsonic and sub-fast. Since the Mach numbers are relatively close to one, it is useful to speak of transalfvénic and transsonic flow. The physics of such cases is particularly complex since none of the three terms in the plasma momentum balance equation, i.e. the acceleration term, the plasma pressure gradient or the magnetic force, can be neglected. The problem is further complicated, because the ion gyroradii are comparable to the radius of Titan R_T. Some of the consequences of these results will be discussed in Sec. V. The deviation of plasma flow leading to an inward flow component may be interpreted in terms of a temporary inward motion of Saturn's magnetopause during the Titan encounter.

TABLE Ia
Incident Magnetoplasma Properties

Magnetic field magnitude B	5 nT
Direction	approximately perpendicular to orbital plane
Plasma flow speed	80–150 km s^{-1}
Plasma speed adopted V	120 km s^{-1}
Plasma flow direction	20° from corotational direction inward
Proton number density n_p	0.1 cm^{-3}
N^+ number density n_{N^+}	0.2 cm^{-3}
Electron temperature $k\,T_e$	200 eV
Proton temperature $k\,T_p$	210 eV
N^+ temperature $k\,T_{N^+}$	2.9 keV
Electron number density n_e	0.3 cm^{-3}

TABLE Ib
Derived Quantities*

Mass density ρ	2.9 amu cm^{-3}
Total plasma pressure p	1.1×10^{-9} dynes cm^{-2}
$\beta = p/(B^2/2\mu o)$	11.1
Alfvén speed V_A	64 km s^{-1}
Sound speed $V_s = 2p/\rho$	210 km s^{-1}
Fast magnetoacoustic speed $(V_A^2 + V_s^2)^{1/2}$	220 km s^{-1}
Alfvén Mach number $M_A = V/V_A$	1.9
Sonic Mach number $M_s = V/V_s$	0.57
Fast Mach number $M_f = V/(V_A^2 + V_s^2)^{1/2}$	0.55
Gyroradius of newly created proton	248 km
Gyroradius of thermal proton	413 km
Gyroradius of newly created N^+ − ion	3470 km = 1.35 R_T
Gyroradius of thermal N^+ ion	5790 km = 2.25 R_T
Gyroradius of thermal electron	9.5 km
Motional electric field $B \cdot V$	0.6 volt km^{-1}

*Titan radius used R_T = 2570 km.

IV. QUESTION OF AN INTERNAL MAGNETIC FIELD OF TITAN

Since the flyby lasted only a few minutes, we use the magnetic field data for a first overview to ensure high spatial and temporal resolution. These data are shown in Fig. 2 for a 30-min interval including the time of closest approach 0540 UT. Close inspection of the highest time resolution data (16 2/3 vectors per second) shows that no information is lost by our choice of 1.92 s averages. The most conspicuous features of Fig. 2 are the various dips in magnetic field magnitude. The deep minimum at 0529 UT and the minor one at 0533 UT are distinct from the sharp minima around closest approach at 0539:29, 0542:29 and 0544:21 UT. At least the deep minimum at 0529 UT has probably nothing to do with the actual interaction. First, the magnetic field direction does not differ appreciably from the direction of Saturn's dipole field at $\sim \delta \approx -90°$ whereas the sharp minima around closest approach are characterized by directions $\delta \approx 0°$, i.e. in Saturn's equatorial plane. Second, the former minimum is not uncommon in the outer magnetosphere of Saturn after the last magnetopause crossing. In fact, the magnetic field behavior typical of the outer magnetosphere of Saturn observed during the Voyager 1 encounter continues to at least 0532 UT and resumes at about 0546 UT. We note that the rapid variations of λ in the earlier part of the interval shown in Fig. 2 are due to magnetic field vectors being close to the south pole of the magnetic vector coordinate system.

Independent evidence to define the specific interaction region can be obtained from the electron data (Bridge et al. 1981*a*; Hartle et al. 1982). Figure 3 shows $\log f_e$ as a function of electron velocity, where f_e is the velocity space electron distribution function for times from 0521 UT to 0554 UT. We note that the measurements in electron mode E_2 begin 44.2 s after the end of E_1 the time which is used in the plot. Two features in Fig. 3 are significant. At low energies we observe a maximum in $\log f_e$ whereas at high energies $\log f_e$ displays a minimum with increasing steepness of the flanks of the minimum towards lower energies. The high-energy behavior is somewhat delayed with respect to the low-energy behavior. As a function of energy or velocity it abruptly stops below 16,000 km s^{-1} or $\sim$ 700 eV. The core of this "bite-out" region lasts from $\sim$ 0538 to 0543 UT, where the times have been corrected for the shift between modes E_1 and E_2. The figure confirms our assertion, that at least the B minimum at 0529 UT is not connected with the actual interaction region. The figure allows an easy deduction of the electron temperature from the width of the distribution.

Our next step is to look for a possible fast bow shock, which would show up as a steep jump in B towards the center of the wake. Careful inspection of Fig. 2 shows no evidence for a fast MHD shock either inbound or outbound. This independently confirms the result shown in Table I, that the fast Mach number M_f is < 1, i.e.

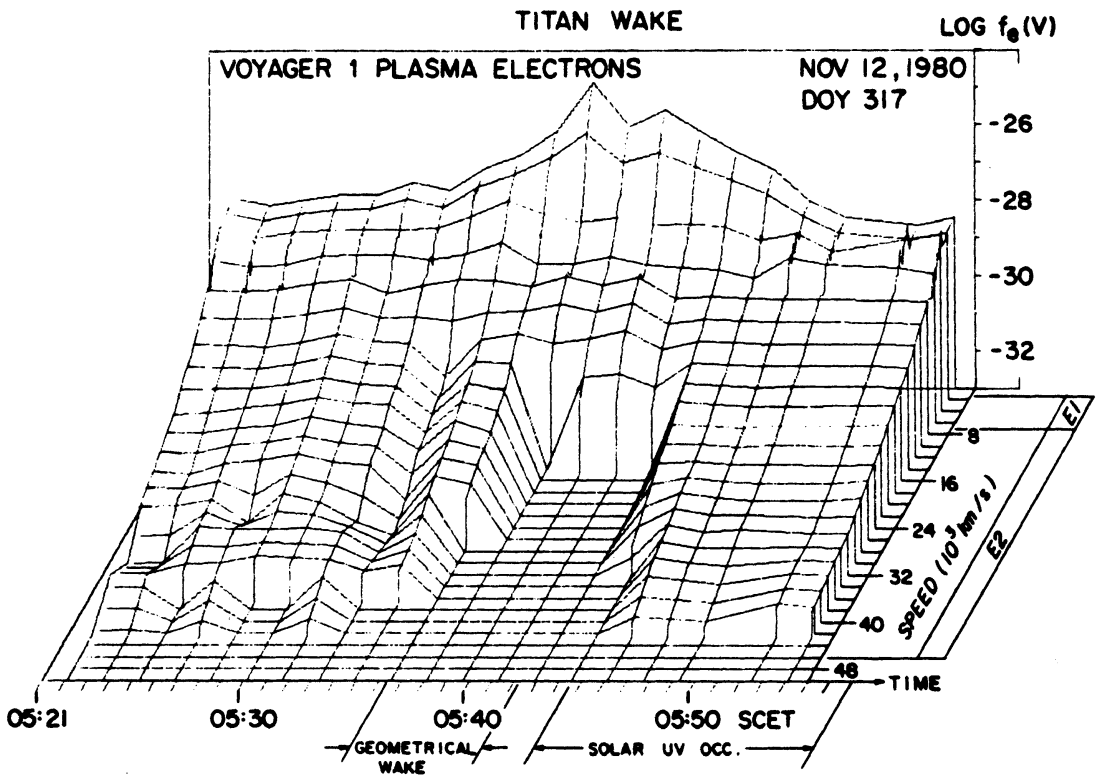

Fig. 3. Electron distribution function f_e as a function of velocity for the Titan encounter period. Note the electron bite-out region above ~ 16,000 km s^{-1} (from Hartle et al. 1982).

$$M_f = \frac{V}{(V_A^2 + V_s^2)^{1/2}} \lesssim 1. \tag{1}$$

Inserting the expressions for V_A and V_s we obtain a useful alternate interpretation of M_f, i.e.

$$M_f = \left(\frac{\frac{1}{2}\rho\, v^2}{p_t} \right)^{1/2} \tag{2}$$

where $p_t = p + B^2/2\mu_0$ is the total pressure.

The question of the identification of an internal magnetic field of Titan depends to some extent on our knowledge of what a magnetosphere in sub-fast ($M_f < 1$) flow would look like. Nothing is known about a magnetosphere under these conditions. Note, that the variation of the magnetic field due to a simple dipole along the trajectory will be appreciably modified by the field of plasma currents. The following discussion has therefore to be taken with a grain of salt.

Let us assume that a magnetosphere in sub-fast flow also develops a magnetospheric tail opposite to the direction of incident flow, with a corresponding cusp region known as the midnight cusp in the case of the Earth. If the magnetic moment of Titan were very strong, the Voyager 1 encounter trajec-

tory would have passed inside the cusp. In this case two magnetopause crossings should have been observed with an approximately dipolar field region in between. Figure 2 shows three dips in magnetic field magnitude and other deviations from the expected behavior, and therefore excludes this possibility.

For a smaller dipole moment the cusp would be located inside the encounter trajectory, that would then pass through the hypothetical magnetospheric tail due to the global magnetic field of internal origin as postulated. If the dipole moment were approximately parallel or antiparallel to the rotational axis of Titan, we would expect a neutral sheet in the equatorial plane of Titan which coincides with its orbital plane. According to the trajectory characteristics described above, we could interpret the first dip in magnitude B as the inbound magnetopause, the second one as due to crossing the neutral sheet of the tail and the third one as the outbound magnetopause. The regions L_1 and L_2 in Fig. 2 are then the northern tail lobe and southern tail lobe, respectively. The magnetic field data can be displayed more clearly by projecting the vectors into the XY-plane and the YZ-plane. Figure 4 shows every fifth 1.92 s average magnetic field vector in this representation. (No significant detail is lost by the decimation.) We see that the vectors in tail lobe L_1 point toward Titan whereas those in L_2 point away from the satellite. The hypothetical di-

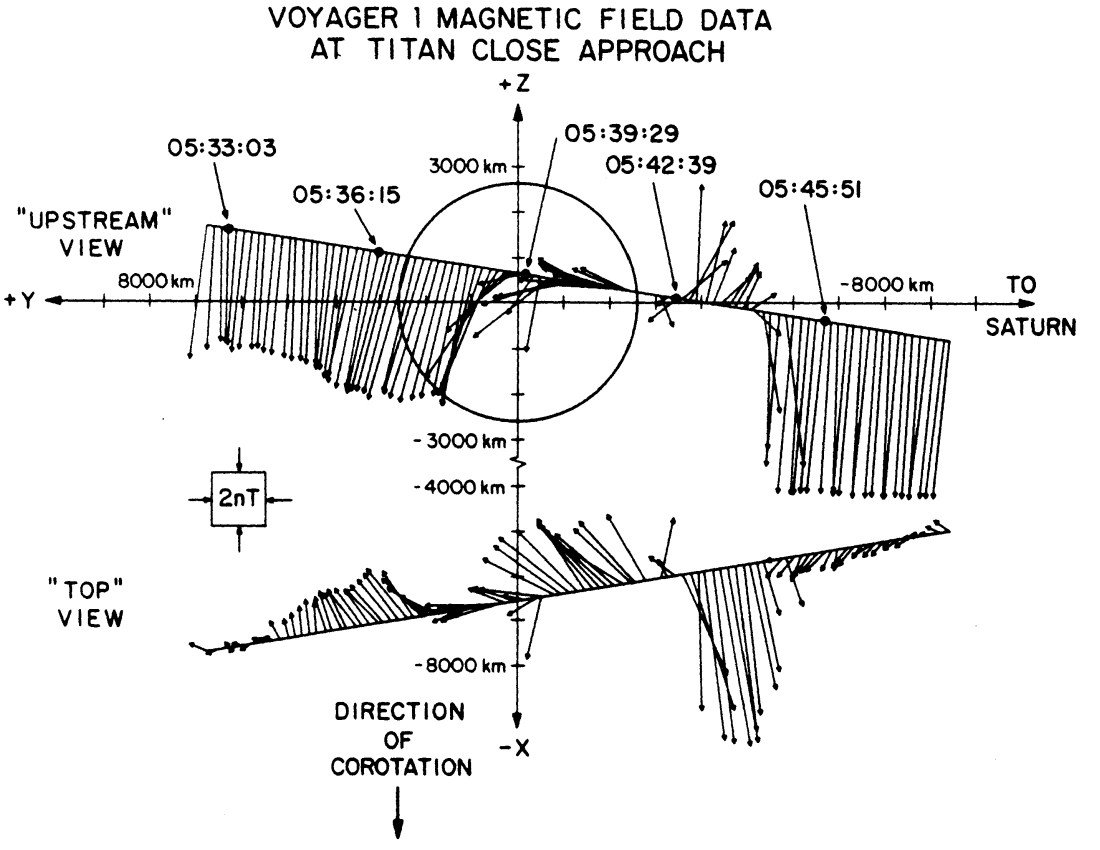

Fig. 4. Projections of magnetic field vectors on YZ and XY planes superimposed on the Titan flyby trajectory. The 1.92 s observations have been decimated by a factor of five (from Ness et al. 1982*b*).

pole moment of Titan would therefore point in a direction antiparallel to the magnetic moment of Saturn. According to present knowledge in this field, reconnection should essentially go on continuously in this case. However, no evidence for hot plasma-sheet electrons is found in the electron data of Fig. 3. On the contrary, a strong reduction of electron temperatures is indicated by the electron observations. In addition, the substantial differences in field magnitude between the two tail lobes are difficult to understand, if they are due to a magnetic field of internal origin parallel or antiparallel to the Z-axis. We can give a very conservative upper limit for an internal field of Titan by attributing the magnetic flux through a tail with a somewhat arbitrary extension of $\pm$ 5 R_T in the $\pm$ Z direction and the observed field along the trajectory to the total flux through one hemisphere. The result is $M \lesssim 7 \times 10^{20}$ Gauss cm^3 corresponding to a surface equatorial magnetic field of $\lesssim 4.1$ nT. The magnetic field is therefore much less than the 100 nT field derived by one of the authors (Neubauer 1978) for the most favorable case for dynamo action. Using Eq. (1) of Neubauer (1978), the upper limit to the radius of an inner metallic core would be 410 km. This upper limit is only significant under the condition that there is enough energy to drive a dynamo, a condition which need not necessarily be fulfilled. The small fraction of Titan's radius, which this upper limit implies, i.e. 0.16, also leads to the expectation, that if a dynamo field exists, it would be dipolar to a good approximation.

In conclusion, there is no evidence for the interaction between Titan and Saturn's sub-fast magnetoplasma being due to an internal magnetic field. Since an extensive atmosphere is known to exist, the interaction must therefore be atmospheric as in the case of Venus with the formation of an induced magnetosphere of the tail which has been traversed by Voyager 1. If an internal field close to our upper limit should exist, there would be some limited influence on the flow system.

V. INDUCED MAGNETOSPHERE OF TITAN

A. Mass Loading and Field-Line Draping

In this section we shall review the interpretation of the encounter data of Voyager 1 in terms of an induced magnetosphere, which relies on the physical concepts of mass loading by mass pickup and magnetic field-line draping. Mass loading and draping are intimately connected when the frozen-in field concept is applicable. Before we can apply these concepts, we must be sure that the frozen-in field concept applies in the case under consideration. The electron gyroradius in Table I indicates that at least the electrons will be frozen to the magnetic field lines down to the level where the collision frequencies approach the electron cyclotron frequency. The large ion gyroradii would tend to allow deviations from the frozen-in field conditions. However, estimates of the current densities based on a simple application of Ampère's law to the magnetic field data combined with typical densities, indicate rela-

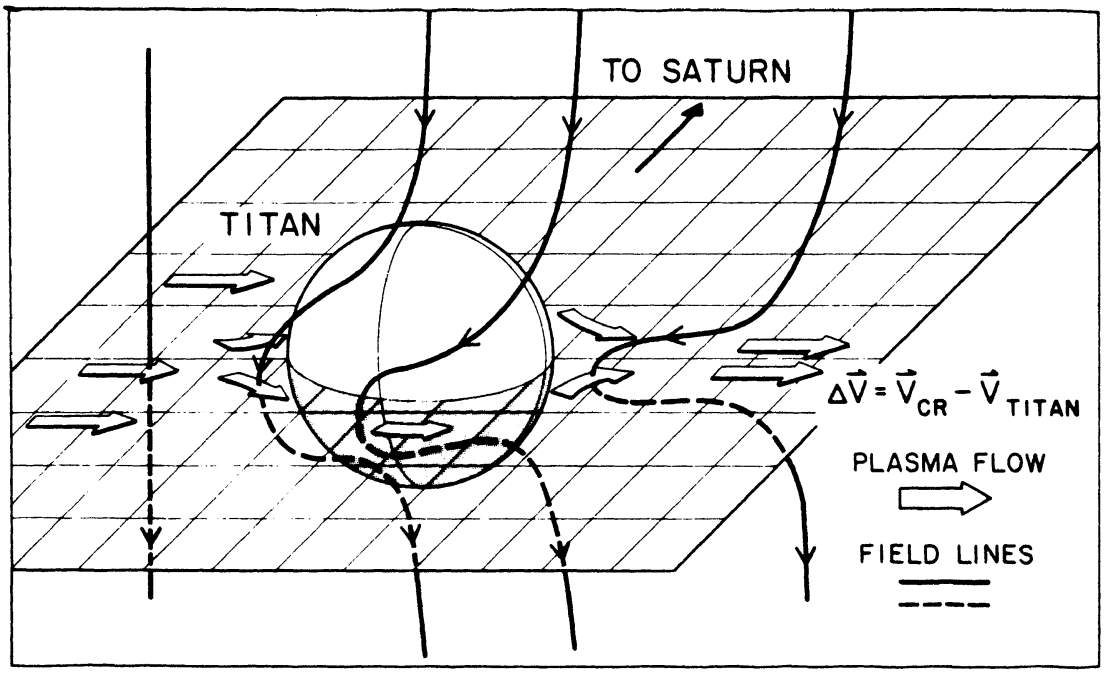

Fig. 5. Sketch illustrating magnetic field-line draping at Titan (from Ness et al. 1981).

tive speeds between ions and electrons which are small enough to constrain the motion of ions to follow the frozen-in field concept in a smoothed-out sense.

In analogy with a comet and the case of Venus, the formation of an induced magnetosphere at Titan can then be described as follows (see Fig. 5). Consider an initially straight flux tube of small diameter along the $(-Z)$ direction filled with the incident plasma, as characterized in Table I, as it moves towards the satellite. Because of the sub-fast character of the flow, the signal in the fast MHD-mode caused by the partial shortcircuiting of the motional electric field by Titan's ionosphere can propagate in all directions and prepare the incident plasma to slow down and deviate around Titan, before collisions with the neutral atmosphere become important. As an initially straight flux tube enters the hydrogen corona of Titan or even the nitrogen dominated atmosphere close to the satellite, mass loading due to the production of electrons and ions in the flux tube will slow down the flux tube near $Z = 0$. In the mass loading or mass pickup process, a newly generated ion is accelerated by the electric field from the small or zero initial velocity of the parent neutral in Titan's frame to a new average velocity corresponding to the $\mathbf{E} \times \mathbf{B}$ drift speed. The necessary momentum is extracted from the flow leading to a decelerating effect. Here the ion production is due to photoionization and collisional ionization by electrons in the high-energy tail, above 700 eV of the magnetospheric electron distribution function having a bulk temperature of 200 eV. Whereas the part of the flux tube near $Z = 0$ is slowed down by the mass loading, it proceeds in an unimpeded way at large values of $|Z|$. In addi-

tion to mass loading, elastic collisions between plasma particles and neutral gas will impede the flow around $Z = 0$ particularly closer to Titan, where elastic collisions become relatively more important. As the mass loading continues, the tip of the flux tube lags more and more behind the unperturbed field line at large $|Z|$. Figure 5 illustrates this process referred to as magnetic field-line draping, first described by Alfvén (1957) in an application to comets. More precisely, the mass loading near $Z = 0$ generates an Alfvén wave signal leading to a bending of the flux tube, as the Alfvén wave propagates up and down the undisturbed flux tube along $+Z$ and $-Z$. The Alfvén wave signals affect a region limited by the Alfvén Mach angles $\tan^{-1}M_A^{-1} = 28°$.

Because of the increased mass density due to the mass loading, the Alfvén speed is relatively small near $Z = 0$ leading to a particularly pronounced stretching of the draped flux tube. As the draped field line enters the wake region, the draping will become stronger and stronger until the tension in the field line pulls it away from the ionosphere. Figures 5 and 6 show the flow in the XY-plane. This tension will eventually lead to an acceleration of the plasma on the field line near $Z = 0$ until the initial velocity is recovered. The tensional force can also be described in terms of a $\mathbf{j} \times \mathbf{B}$ force with $\mathbf{j}$ being directed along $+Y$. Since the overall current system must be source-free, there must also be a system of Alfvénic currents (Drell et al. 1965; Neubauer 1980; Goertz 1980; Eviatar et al. 1982) towards the plane $Z = 0$ at negative Y and away from $Z = 0$ at positive Y. This has been displayed schematically in Fig. 9 in Sec. V.D.

If we compare our case with Venus, we expect the flux tubes penetrating deepest into Titan's atmosphere to be finally guided around the satellite along an ionopause boundary layer. At this boundary there is total pressure equilibrium between the outer mass-loaded, stretched-out magnetic field and the inner ionosphere of Titan, which is due to ionization by solar extreme-ultraviolet (EUV) photons and collisional ionization by high-energy charged particles with gyroradii big enough to penetrate the boundary. The distance of this boundary from Titan has been estimated at 4400 km by Hartle et al. (1982) for the day side. We also mention here, that the formation of an ionopause layer is not always possible. If the ionization inside any assumed ionopause is insufficient, e.g. due to very low EUV-photon fluxes to produce enough pressure to balance the mass loaded plasma, we expect a gradual decrease in velocity with field lines even penetrating to the inside of the ionosphere.

Taking the electron density to be 3×10^3 cm^{-3} in the ionosphere of Titan (Strobel and Shemansky 1982), a temperature sum $T_e + T_i = 4600$ K is necessary to balance the estimated ram pressure using the parameters in Table I. An ionopause should therefore exist at least around part of Titan's atmosphere-ionosphere system. Upper bounds of 3×10^3 cm^{-3} and 5×10^3 cm^{-3} on the electron density have been derived by Lindal et al. (1983) near the evening and morning terminators, respectively.

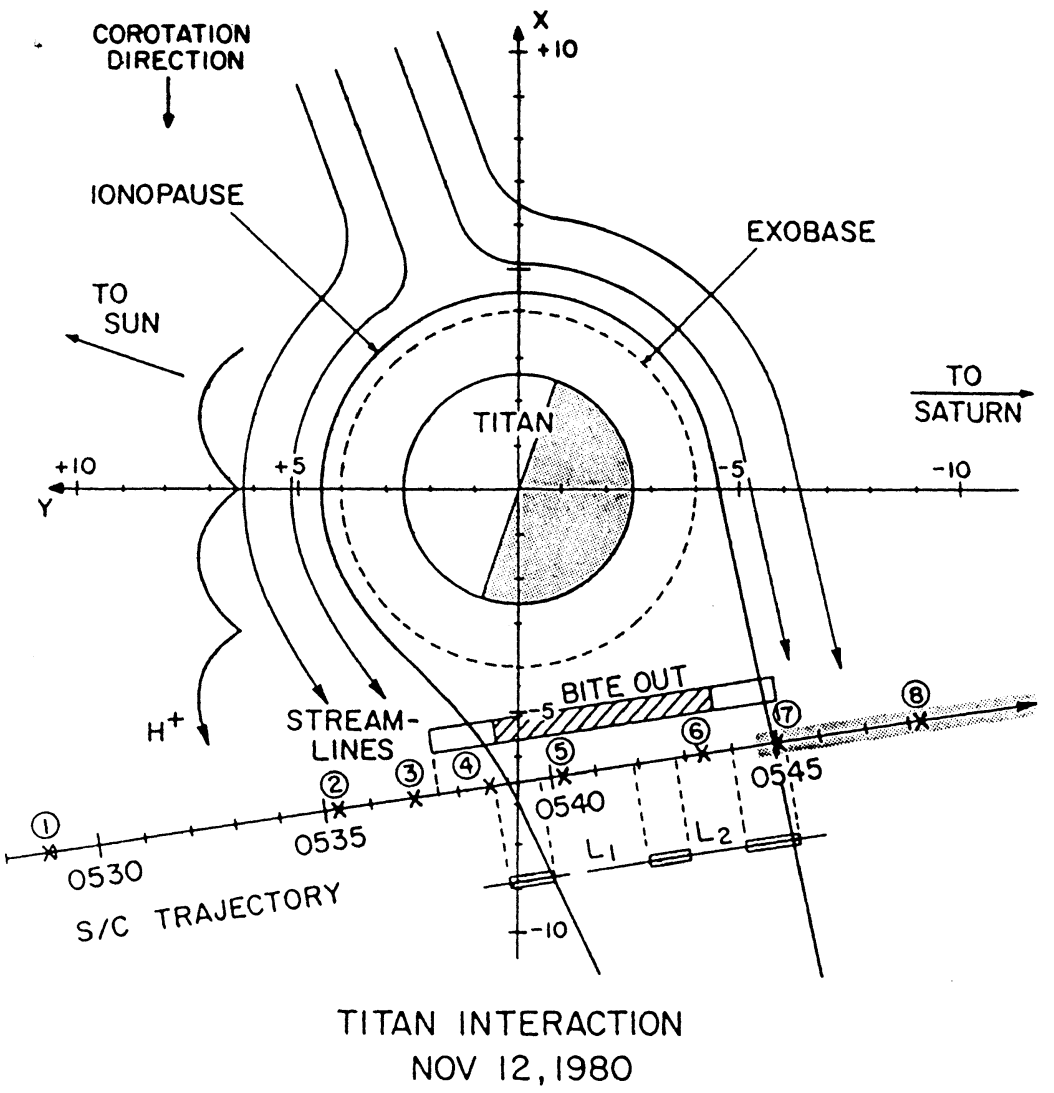

Fig. 6. Idealized plasma flow around Titan. L_1 and L_2 refer to the northern and southern magnetic tail lobes. The shaded bars refer to the minima corresponding to magnetopause and neutral sheet crossings. The trajectory of a proton is approximately to scale in the observed magnetic field (after Hartle et al. 1982).

The draping picture described above suggests, that the magnetic field projected into the *XY*-plane has a component towards the flow north of the equatorial plane and a component parallel to the flow south of it, i.e. at $Z < 0$. This expectation is born out by information in Fig. 4, since the spacecraft was first north and after 0543:07 UT south of the equatorial plane. Starting at 0533 UT the magnetic field begins to develop a projection towards the direction of incident flow in the *XY*-plane while the total vector is predominantly in the southern direction. Then the *XY*-projection starts to rotate in a counterclockwise sense, until at about 0538:30 UT the total vector suddenly begins to rotate completely into the *XY*-plane. In the *XY*-plane after further clockwise rotation, it is first directed essentially antiparallel to the incident flow direction, as expected for draping north of the symmetry plane in Fig. 5. After 0542:39 UT the field is directed roughly parallel to the direction of incident

TABLE II
Results of Analysis of Ion Spectra

Numbers in Fig. 6	Ion Species / Time Interval 05, SCET	H^+			N^+			N_2^+/H_2CN^+		
		V, km s^{-1}	n, cm^{-3}	kT, eV	V, km s^{-1}	n, cm^{-3}	kT, eV	V, km s^{-1}	n, cm^{-3}	kT, eV
4	38:35–38:39	60	2.5	2.1	10	15	2.1	5	30	2.1
5	40:11–40:15	25	1.9	3	5	7	1.8	3.5	10	0.9
6	43:23–43:27	50	1	3	10	3	2.1	4	10	2.4
7	44:59–45:03	40	1	33	20	22	29	—	—	—

flow, comparable to the draping south of the symmetry plane in Fig. 5. The switch in the magnetic field direction in the *XY*-plane from antiparallel to parallel to the direction of incident flow is almost exactly coincident with the crossing of Titan's equator. At about 0544:30 UT the strong southerly component appears again with a relatively small component parallel to the incident flow direction. We can therefore distinguish a region of weak draping with predominantly southerly fields surrounding a region of strong draping near Titan with fields in the *XY*-plane.

Let us now discuss the consequences of the mass pickup process by use of the plasma science observations on the encounter trajectory. As we approach Titan, the weak draping region can be attributed to the pickup of protons in Titan's hydrogen corona. The subsequent transition from weak to strong draping is consistent with the onset of heavy ions (N^+ or N_2^+/H_2CN^+) of ionospheric origin. The observed energy spectra of these ions are increasingly consistent with the pickup energy distribution expected for newly ionized neutral gas (cf. Hartle et al. 1982, their Fig. 4; Hartle et al. 1973). This provides a direct experimental association of the observed plasma in the wake with processed portions of Titan's neutral atmosphere, and indirectly implies copious momentum exchange, as the mass loading of newborn ions slows the incident magnetized plasma. The results of fitting convected Maxwellians to the ion data in and near the region of strong draping are given in Table II. The locations on the encounter trajectory are also indicated by the numbers four to seven in Fig. 6. As will be shown in Sec. V.B, where electron densities consistent with all data are derived, the heavy ion interpretations must be considered the realistic ones. The fits then clearly define a strong shear layer between at least 0537 and 0539 UT with the plasma moving only 5 to 10 km s^{-1} just before the dip in the magnetic field preceding the region L_1 in Fig. 2, indicating the inbound magnetopause. This should be contrasted with the 80 to 150 km s^{-1} flow observed in the undisturbed magnetosphere of Saturn. The analysis of observed low-energy charged particles by Maclennan et al. (1982) suggests an even earlier onset of the low-velocity region indicating the shear layer.

Throughout the inbound velocity shear layer the electrons collected by the plasma science instrument are observed to cool as a result of the addition of cold electrons which are the by-products of the ionization process. This has already been noted in connection with Fig. 3. The electron velocity distributions f_e through this region begin to show evidence of inelastic interactions (e.g., electron impact ionization) of the hot magnetospheric plasma with neutral gas, where the strong bite-out region lasts for the entire duration of the strong draping region as defined by the magnetic field.

The ion analysis is consistent with a neutral exosphere model, which has N_2 as the dominant molecule above the exobase at 4000 km with a transition to a hydrogen-dominated exosphere at 5000 km. The exobase temperature has been taken to be 160 K (Hartle et al. 1982).

B. Electron Density Variation in Titan's Wake Along the Voyager 1 Encounter Trajectory

The important variation of total electron density can only be obtained by a synthesis of the plasma science electron and ion data and the wave data obtained by the plasma wave and planetary radio astronomy experiments. We shall use Fig. 7 to develop the solutions, which will also indicate the complexity of distribution functions resulting from magnetoplasma-atmosphere interactions.

First, the electron densities obtained by the plasma experiment in modes E_1 and E_2 are shown by octagons. They are based on direct integration of the electron distribution function f_e observed above 10 eV and approximated by a Maxwellian fit to the lower energy channels for energies < 10 eV. We may use the term hot electrons for these electrons in contrast to a distinct cold electron population at energies well below 10 eV which coexists with hot electrons, as we will argue later in this section. The corresponding densities and temperatures can be called n_H, n_c and T_H, T_c, respectively. Figure 7 indicates a maximum in n_H in the shear layer which is combined with a minimum in the temperature T_H, also suggested by Fig. 3. The temperature T_H is cooler than the magnetospheric value throughout the entire region of draping. The strong bite-out region is also indicated in the upper panel of Fig. 7. The lighter stippling reflects the temporal uncertainties of these boundaries.

The plasma science ion data, part of which are given in detail in Table II, give a first hint that electrons are hidden outside the energy range of 10 to 6950 eV. The electron densities required to balance the ion densities under the three assumptions H^+, N^+, N_2^+/H_2CN^+ are also shown in Fig. 7 and turn out to be greater than the densities n_H.

The additional use of the electron density information contained in the observation of upper hybrid resonance (UHR) emissions allows the reconstruction of the total electron density. UHR emissions occur, when a cold electron component of density n_c exists together with a hot, loss-cone type electron distribution of density n_H under suitable conditions of the temperatures T_c and T_H and other parameters. For a thorough discussion we refer the reader to Hubbard and Birmingham (1978) and Birmingham et al. (1981). In the important special case $n_c >> n_H$ the UHR emissions occur at $f_{UHR} = (f_{pc}^2 + f_{ce}^2)^{1/2}$ where f_{pc} is the cold plasma frequency given in Hertz by $f_{pc} = 9 \times 10^3 \cdot (n_c)^{1/2}$ with n_c in electrons per cm^3 and f_{ce} the electron cyclotron frequency given by $f_{ce} = 28$ Hz $\cdot B$ where B is given in nanoteslas. Hence f_{UHR} yields n_c or because $n_H << n_c$ approximately, the total electron density $n_e = n_c + n_H \approx n_c$. For $B \lesssim 7$ nT and $f_{UHR} \gtrsim 5.62$ kHz we always have $f_{ce} \lesssim 196$ Hz and therefore $f_{UHR} = (f_{pc}^2 + f_{ce}^2)^{1/2} \approx f_{pc}$, i.e., the frequency scale f_{UHR} can immediately be turned into a density scale for n_c. If $n_c >> n_H$ is not fulfilled, the relationship between f_{UHR} and the densities n_c or n_H is more complicated (Hubbard and Birmingham 1978), although n_c generally is the directly determined quantity.

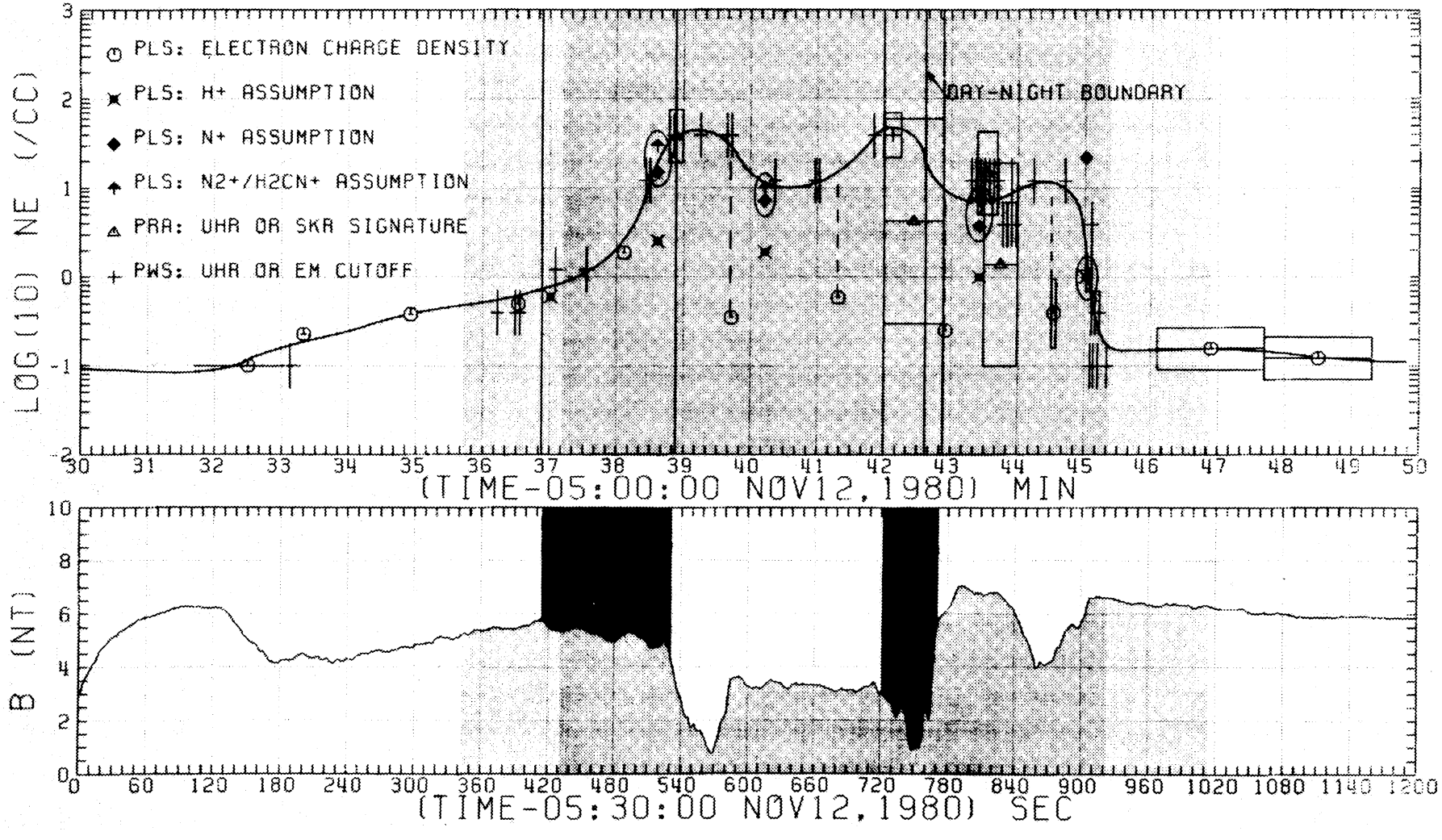

Fig. 7. Voyager Titan wake encounter. Electron densities from various experimental sources are indicated (PLS, PWS, PRA). For a detailed discussion see text. The solid curve represents total electron density consistent with the data and physical concepts developed in this chapter. The magnetic field magnitude and PRA drop-out regions are also shown for guidance.

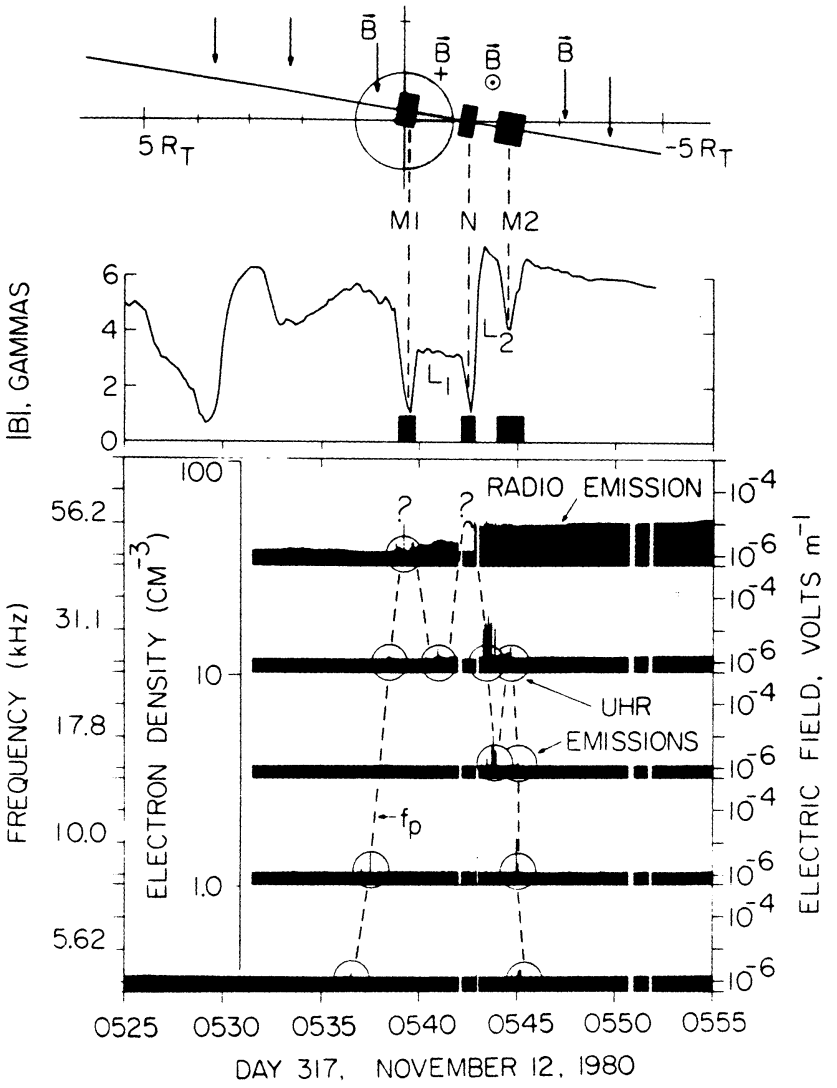

Fig. 8. Observations of upper-hybrid resonance (UHR) emissions and Saturn radio emissions in the upper frequency range of the Voyager plasma wave experiment (after Gurnett et al. 1982*b*).

Let us now briefly discuss the plasma wave observations relevant to this problem. They are shown in Fig. 8 for the frequency channels from 5.62 kHz to 56.2 kHz. Gurnett et al. (1982*b*) point out that the UHR emissions are excited as a narrowband emission near the local f_{UHR}. In addition to the upper hybrid resonance emissions we also observe nonlocal radio emissions from Saturn, the observation of which requires both the activity of the source and an unobstructed path of propagation. The possibility, that these emissions may be generated in Titan's vicinity (Gurnett et al. 1981*a*), has been ruled out by Daigne et al. (1982). Since the identification of the UHR emissions depends to some extent on their burst-like character, it is generally not difficult to distinguish local UHR emissions and nonlocal Saturn radio emissions, except for cases when the latter are very intense or the propagation path connecting the source with the spacecraft varies rapidly. The observed candidates for UHR emissions are encircled in Fig. 8. The question marks indicate possible exten-

sions to even higher frequencies or densities. The first density maximum at 56.2 kHz is derived by one UHR spike only indicating the maximum f_{UHR} to be contained in the channel corresponding to a maximum density of ~ 40 cm^{-3}. The second density maximum at about 0542:30 UT could be as high as ~ 60 cm^{-3} according to combined plasma wave and planetary radio astronomy data. We shall come back to this point later (Sec. V.C). A third maximum of 12 cm^{-3} occurs in the electron density determined from the UHR emissions at about 0544:30 UT.

Let us now return to Fig. 7. The electron densities derived from the upper hybrid resonance (UHR) frequencies observed by the plasma wave (PWS) experiment are shown by vertical-horizontal crosses. The planetary radio astronomy (PRA) data are shown as open triangles. There are appreciable differences between the plasma science (PLS) electron densities and the PWS-PRA set of inferred values. However, the times of the measurements agree in only one case, when the PLS electron data were obtained in the low-energy mode E_1 lasting from 0539:42 to 0539:43.9 UT. However, the reliability of the relevant UHR data point could be questioned since the corresponding spike occurred at a time when Saturn radio emissions start to appear and UHR emissions start to move from 56.2 kHz to 31.1 kHz. It may therefore be due to intensity scintillations of 56.2 kHz Saturn radio waves, as the source rises above some plasma horizon as seen from the spacecraft. Note that no corresponding spikes are seen at the frequency of 59 kHz by the PRA experiment. Apart from this one possible point, we could in principle explain the differences between the PLS electron densities and the UHR densities as being due to temporal or, better still, to spatial variations in density. To be consistent with the physical models for the generation of UHR emissions (Hubbard and Birmingham 1978), this electron population would then have to be called the cold population whereas a hot destabilizing population would have to be postulated at temperatures above 6.95 keV. In other words, in this interpretation the PLS measurements have fortuitously missed the times of high electron densities. Although we cannot completely exclude this possibility, we prefer an alternate explanation because of general considerations of the physics involved. As suggested by Gurnett et al. (1982*b*) and independently by physical arguments, in this interpretation the electron population, resulting from a relatively strong interaction between the plasma and Titan's atmosphere (see chapter by Hunten et al.) and delineated by the core of the electron bite-out region, contains a cold ionospheric part at energies well below 10 eV, the lower energy limit of the PLS experiment. The electrons observed by the PLS-sensor in this strong interaction region, approximately coinciding with the region of strong draping, must be considered as a mixture of cooled magnetospheric electrons, secondary electrons resulting from collisional ionization and photoelectrons. The PLS electrons are then the hot electrons responsible for the UHR emissions. They can be characterized by the density n_H and temperature T_H. Since the UHR emissions require loss-cone type distri-

butions, the values of n_H in Fig. 7 contain a small systematic error because of the isotropy assumption in deriving them. The PWS-PRA densities then correspond to the cold electrons characterized by n_c and T_c in the region of strong draping. Outside this region the condition $n_H \ll n_c$ is less well fulfilled and the assignment of n_c to the PWS densities is less accurate. Gurnett et al. (1982*b*) have estimated an ionospheric temperature of 8600 K by assuming total pressure equilibrium in the tail of the induced magnetosphere, which coincides with the strong draping region. Analysis of the response of the PLS instrument to a cold electron population of 8600 K shows that the densities required by the PWS observations are completely consistent with the PLS data.

We have also drawn a solid line in Fig. 7 which expresses our preferred total electron density variation. The vertical dashed lines represent the cold ionospheric densities not seen by PLS. The ion data shown by solid symbols in Fig. 7 nicely fit into this picture, if we assume the heavy ions N^+ or N_2^+/H_2CN^+ to be dominant in the strong interaction region, except for the time 0545 UT (Hartle et al. 1982). We have therefore emphasized these data points. Unfortunately, the three possibilities regarding the composition cannot be distinguished.

Let us finally turn to the electron densities beyond the dip in B terminating the magnetic lobe L_2 in Fig. 2, which in our picture of the induced magnetosphere of Titan will be termed the outbound magnetopause crossing. The electron densities above the night side of Titan after about 0545:30 UT do not show a gradual falloff but drop immediately to magnetospheric densities. This is also consistent with Fig. 3 and the reduced plasma sheath noise in Fig. 10 that will be discussed in Sec. V.E. The smaller extent of mass loading on the night side may be due to a less pronounced hydrogen corona above the night side due to much cooler atmospheric temperatures. The less pronounced draping in the magnetic field of Fig. 4 after 0545:30 UT may be due to this diminished mass loading but could also be explained by a closer distance to the symmetry plane of the draped field lines, that may have moved in the $(-Z)$ direction. Also we mention, that the electric field direction is such that newly formed ions are accelerated into the dense atmosphere on the night side and away from it on the day side (Bridge et al. 1981*a*).

C. Magnetopause and Neutral Sheet Boundaries of the Induced Magnetosphere and Associated Density Structure

After having reviewed the observations along the Voyager 1 encounter trajectory and their interpretation in terms of mass loading and draping, we shall now describe the resulting structure in three dimensions. The induced magnetosphere is bounded by a plasma layer, which may be referred to as the magnetopause. The magnetopause is produced by draped field lines that get their mass load in the transition layer from the H^+ loading region to the N^+ or N_2^+/H_2CN^+ loading region; in our model this region corresponds essentially to the transition from the outer weak draping region to the inner strong drap-

ing regime. Here high-plasma densities develop in the mass loading process, which are dragged away from Titan by the draped field lines. As the plasma moves outward, it adjusts to the smaller surrounding total pressure. It accomplishes this by an expansion leading to approximate pressure equilibrium with the surrounding plasma and a reduction of the frozen-in magnetic field strength; this results in boundary layers of minimum magnetic field downstream of the dayside and nightside atmosphere of the satellite. The Voyager 1 spacecraft crossed the inbound magnetopause around the central time 0539:29 UT and the outbound magnetopause about 0544:21 UT. We have noted the associated dips in magnetic field magnitude in Fig. 2 and the maxima in plasma electron density in Fig. 7. The important orientation of these magnetopause boundaries almost perpendicular to the *XY*-plane has been shown by detailed analysis of the transition data within the boundaries (Ness et al. 1982*b*). The duration of the magnetopause crossings was 59 s and 79 s for the inbound and outbound magnetopause, respectively; this leads to thicknesses of 1000 km and 1350 km, respectively, if we use the projection of the flyby speed on the *XY*-plane. Following arguments proposed by Daigne et al. (1982), we can even infer the density structure of the inbound magnetopause away from the trajectory. These authors have shown from the drop-out of Saturn radio waves, that the electron density of 40 cm^{-3} extends to a level of 150 km above the spacecraft trajectory corresponding to $Z \approx 0.25\ R_T$. A decrease in electron density away from $Z \approx 0$ is expected, since in a draped magnetic flux tube the plasma accumulates near the tip of the tube at $Z = 0$.

The field lines, that have penetrated into the atmosphere most deeply, are observed well inside the induced magnetosphere. Here draping is essentially complete and the field lines are well aligned with the *XY*-plane. The neutral sheet, which is approximately parallel to the *XY*-plane, then divides field lines with a direction towards the flow in the north and approximately aligned with it in the south. The neutral sheet has been observed around 0542:29 UT with an associated maximum in electron density given by the UHR emission observed by the PWS instrument. Since the grazing incidence hypothesis suggested (see Fig. 6 in Daigne et al. 1982) requires very special conditions, (i.e. a smooth density isocontour without any corrugations and a very special tilt angle), we prefer a blockage interpretation that leads to higher densities in agreement with the PWS data. Our discussion has also provided information on the electron density above and below the Voyager 1 trajectory, i.e., in two dimensions. In this picture maximum electron densities are associated with the magnetopause and neutral sheet boundaries. The minima in density between the boundary crossings in Fig. 7 are then due to a maximum distance from any of the boundaries inside the induced magnetotail.

The approximate picture of the electron density distribution, which for singly ionized ions corresponds to the ion number density distribution, allows us to estimate the mass loss from Titan through its induced tail. From Figs. 4 and 6 a width of 2.5 R_T can be deduced for the induced tail inside the velocity

shear layers mentioned above. The discussion above suggests an extent of ± 0.25 R_T of the major region of mass loss perpendicular to the *XY*-plane. From Table II and Fig. 7 we have estimated an average flux density of 5×10^6 cm^{-2} s^{-1}. This leads to a total loss of $\sim 10^{24}$ ions per second from Titan's atmosphere; the ions would be N^+ or N_2^+/H_2CN^+. The uncertainties are such as to allow even somewhat higher loss rates. This should be compared with other atmospheric loss rates (see e.g. chapter by Hunten et al.). Strobel and Shemansky (1982) also have given a N atom escape rate due to electron impact dissociation of N_2 molecules of 3×10^{26} s^{-1} and an H atom escape rate of 2×10^{26} s^{-1}.

D. Flow Asymmetry and the Picture of Four Tail Lobes

Some additional features of the encounter observations warrant explanations. First, the center of the disturbance region is somewhat offset from the plane $Y = 0$ which would be the symmetry plane for ideal corotational flow and an ionosphere symmetric with respect to the plane $Y = 0$. This may be partly explained by the 20° deviation of the flow and in addition, by the asymmetry of the two lobes of the induced tail.

Since the solar direction, which controls the photochemistry of the ionosphere, is at a large angle to the general direction of incident flow, there will be a strong asymmetry between the parts of the tail lobes resulting from field-line draping around the dayside hemisphere and the nightside hemisphere. The direction of incident flow combined with the 1330 local time yields $90 - 20 - 22.5 = 47.5$ for the angle between the incident flow direction and the solar direction. This also provides an explanation for the maximum of the ultraviolet nitrogen emissions (Strobel and Shemansky 1982) in the quadrant of the sunlit hemisphere facing the ideal corotational flow. The ionization rate will be obviously greater on the day side. As already mentioned, newly created ions will move out of the atmosphere on the day side and run into the deeper atmosphere on the night side because of the sense of gyration determined by the southward magnetic field (Bridge et al. 1981*a*).

As illustrated in Fig. 9 we expect to find a north-south trending boundary or vertical boundary (with respect to the *XY*-plane) in the tail between field lines due to dayside draping and nightside draping. This is in addition to the east-west trending or horizontal boundary (with respect to the *XY*-plane) between northern and southern field polarities produced by the draping and referred to as the neutral sheet. As a consequence we have four tail lobes, which must be carefully distinguished. Since the two dayside lobes (northern and southern) are expected to be loaded with much more plasma than the nightside lobes, some expansion of its magnetoplasma will occur on the day side to enforce total pressure equilibrium across the tail. This will lead to a reduction in magnetic field magnitude in lobe L_1 as observed in Fig. 2. A casual inspection of Figs. 1 and 4 might suggest that the spacecraft crossed the intersection between the day-night boundary and the north-south boundary simultane-

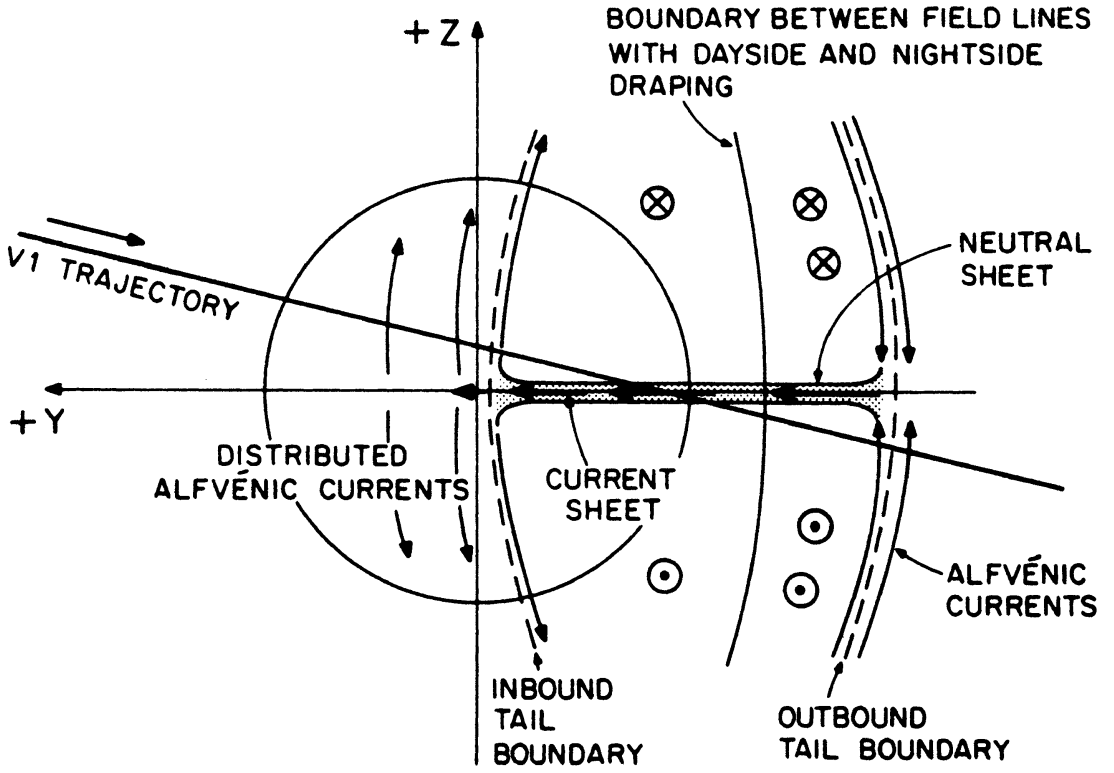

Fig. 9. Four tail lobe picture developed from Voyager 1 magnetic field observations. The sketch also shows the current distribution consistent with the magnetic field topology. The view is towards the direction of idealized corotational plasma flow (from Ness et al. 1982*b*).

ously. This would seem very improbable. However, a close inspection of Figs. 2 and 4 shows that the low magnetic field of lobe L_1 characteristic of the dayside lobe extends somewhat into the southern lobe after the neutral sheet crossing. Voyager 1 has therefore traversed the following tail lobes: northern dayside, southern dayside and southern nightside, where the latter two correspond to L_2 in Fig. 2. A north-south asymmetry could also be expected due to seasonal variations in Titan's atmosphere-ionosphere system (B. A. Smith et al. 1981; Hanel et al. 1981; chapter by Hunten et al.). Five months before the encounter the Sun had passed above the equatorial plane. The above considerations show that both the offset and the asymmetry between L_1 and L_2 can be explained by the atmospheric interaction model. Although the various electron density data cannot resolve the difference between the neutral sheet and day-night boundary, we have schematically indicated in Fig. 7, what one might expect.

E. Dynamical Phenomena

The physical model developed organizes so many data, that it can be expected to be basically correct. However, much more work will be required to understand the interesting dynamical phenomena which are briefly reviewed here.

An interesting feature of the magnetic field data begins at about 0537:00 UT and lasts until 0539:30 UT. If we consider the sequence of magnetic field

vectors as due to some stationary structure, they could be extrapolated to correspond to a clockwise rotation of magnetic field vectors on circles around a fixed axis. Both the assumption of stationary structure and the continuity of vectors around a circle are not much more than plausible working hypotheses. The feature could be explained as due to a bulging of stream lines due to severe deviations of the flow from symmetry (see Fig. 11 in Ness et al. 1982*b*), local vortices in the flow or Titan's counterpart of auroral curls which are characterized by parallel magnetic field and current density in the polar magnetosphere of the Earth (e.g. Hallinan 1976).

Another interesting dynamic feature occurs in the same general region. An oscillation with a fixed period of 33 s occurs in the magnetic field magnitude as indicated by small vertical arrows in Fig. 2 between 0536:50 and 0541 UT. It is interesting to consider the possibility of these oscillations as due to the shedding of vortices in a hypothetical vortex strait following Titan.

The plasma wave experiment showed a number of interesting wave phenomena. Figure 10 shows the encounter observations from 10 Hz to 1000 Hz for the time interval from 0525 to 0555 UT. Two types of broadband wave emissions have been detected. The so-called sheath noise occurs in the inbound region of hydrogen mass pickup where we also observed weak draping of magnetic field lines. As illustrated by Fig. 9, the pickup current in the Y direction decreases with increasing Y, which requires a discharge of the current by Alfvénic currents in the $+Z$ direction. This is confirmed by a straightforward application of Ampère's law to the field projections into the XY plane. However, in addition to the proposal by Bridge et al. (1981*a*), who postulate waves due to the unstable ion distributions produced by the mass pickup process (i.e., essentially rings in velocity space), we propose that these waves may also be due to the approximately field-aligned currents, which generate electrostatic emissions as the auroral electrostatic turbulence reported by Gurnett and Frank (1977).

The so-called tail noise can be considered a similar type to that observed in the magnetospheric tail of the Earth (Gurnett et al. 1976). The mechanism of this type of emissions is not well understood and therefore the diagnostic value here is somewhat limited. There seems to be a sharp change in intensity in the region of the day-night boundary of draped field lines.

F. Relevant Future Investigations

It would be interesting to learn whether effects of the interaction between Titan and its plasma environment have been observed by other spacecraft. One might also look for other examples in the solar system, where at least some of the physical aspects of the interaction problem have been studied in some detail.

Jones et al. (1980) have reported a possible magnetic wake in connection with a bow shock of Titan during the Pioneer 11 encounter of Saturn. Since the fast Mach number in our case was $M_f = 0.55$, a corresponding variation in

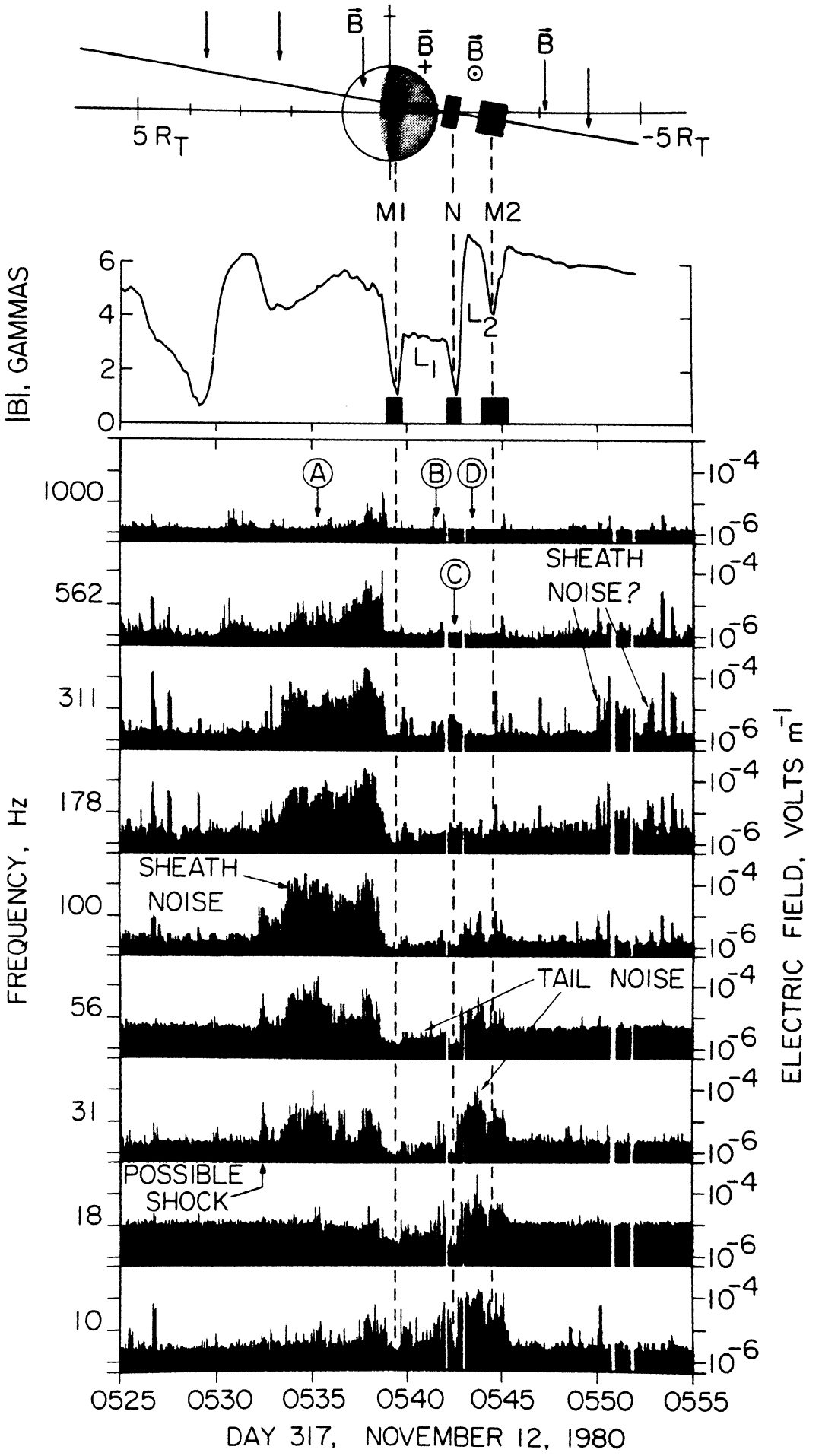

Fig. 10. Plasma wave observations in low-frequency range of the plasma wave experiment (from Gurnett et al. 1982*b*).

plasma and magnetic field parameters to explain $M_f > 1$ is certainly possible. Although the distinction between a Titan wake and some magnetospheric disturbance of different origin is difficult to make, the possibility remains interesting.

Another way to learn more about the interaction is to study some aspects of the physics in similar cases. Atmospheric interactions at Io and Venus have also been studied; we have already used the analogy with Venus in several instances. At Io the Mach numbers turned out to be $M_A = 0.15$ (Acuna et al. 1981*b*) and $M_s = 3.0$ (Bagenal and Sullivan 1981); the case is therefore sub-fast as at Titan. The ordering of the bulk kinetic, magnetic and thermal energy densities is different, however. In Io's case the magnetic field energy density dominates whereas in the case of Titan the plasma thermal energy is dominating although not very strongly. At Io the analysis showed the existence of an Alfvén wing or Alfvénic current tube (Drell et al. 1965; Neubauer 1980; Goertz 1980) carrying a current of 2.8×10^6 amperes driven by a voltage of 500,000 volts across Io (Acuna et al. 1981*b*). In the case of Titan we also expect the existence of Alfvén wings but carrying a much smaller current due to the modest driving voltage of 4800 volts across the diameter of the exobase. At small Mach numbers $M_A < 1$ the Alfvénic currents can be clearly distinguished at large $|Z|$, whereas in our case of $M_A = 1.9$ their disturbance field is expected to merge with disturbances due to the slow magnetoacoustic mode. In the case of Venus, Mach numbers of $M_A \approx 8$ and $M_s \approx 8$ are typical leading to strong bow shocks (Russell et al. 1981) in contrast to the sub-fast case of Titan. However, the effect of the fast Mach number should not be very large above the hemisphere of plasma incidence, since the shock decelerates the plasma to sub-fast speeds $M_f < 1$. The difference is expected to be substantial in the tail region in the case of Venus because of the acceleration of the flow to fast speeds along the flanks of the tail.

At Venus the process called draping has first been studied in detail by *in situ* observations and found to yield a good description of the magnetic field configuration in the wake in terms of an induced tail with a tail neutral sheet perpendicular to the magnetic field frozen into the incident plasma (see e.g. Luhmann et al. 1981). For Venus the atmosphere seems to be much harder than at Titan in the sense of a small ratio scale height/radius at Venus compared with Titan; Titan turned out to be a much softer target than Venus at least as far as dayside conditions are concerned. In this sense the case of Titan's day side is intermediate between the case of Venus and that of a cometary interaction (Biermann et al. 1967; Wallis 1973). The Venus solar wind interaction has recently been compared with Titan's magnetospheric interaction by Kivelson and Russel (1983).

VI. SUMMARY AND CONCLUSIONS

The Voyager 1 encounter of Titan has yielded a unique set of magnetic field, plasma and plasma wave data which allows a first attempt to develop a

comprehensive picture of the interaction between the magnetospheric plasma of Saturn and the atmosphere of Titan. This is complicated by the large angle between the solar direction and the direction of incident flow, the large ion gyroradii and the transsonic and transalfvénic character of the incident flow. A 3-dimensional sketch of the induced magnetotail of Titan as observed during the Voyager 1 encounter and reviewed in this chapter is shown in Color Plate 4. The exosphere of Titan is depicted in blue. Ionization of the upper atmosphere of Titan and the associated mass-loading of magnetic field lines and field-line draping define two regions of enhanced plasma density due to dayside and nightside draping. The boundaries of these regions are shown in red and green, respectively. Note the much more extended dayside draping region due to hydrogen ionization. The figure also gives views of the four tail lobes mentioned above. Whereas the structure near the equatorial plane separating northern and southern lobes has been obtained by data analysis, the north-south boundaries of the lobes have been inferred by more theoretical arguments. Cuts through the enhanced plasma regions are shown cross-hatched. The boundary between the dayside and nightside tail lobes is shown in gray. Several thin magnetic field filaments have also been drawn to illustrate the draping process.

Ideally a physical problem is considered solved, when a quantitative model explaining in detail the observations has been developed. As shown in this review, Titan's magnetospheric interaction is certainly one of the most complex problems among the many possibilities for the interaction between a planetary body and the surrounding plasma environment. For example, an unanswered question is the contribution of Titan's magnetospheric interaction to the energy balance of the atmosphere in view of the power dissipation rate of 5×10^9 W by magnetospheric electrons (Strobel and Shemanski 1982). Although first estimates concerning the processes involved have been published (Eviatar et al. 1982), a comprehensive model may not be available for some time.

Acknowledgments. The results reviewed in this chapter have essentially been derived by a collaborative effort between the Voyager magnetometer, plasma science, plasma wave and radio science teams. We acknowledge the support and significant contributions of the principal investigators N. F. Ness, H. S. Bridge and F. L. Scarf. In addition we acknowledge the particular contributions of our colleagues M. H. Acuña, S. K. Atreya, K. W. Behannon, J. W. Belcher, G. Daigne, M. D. Desch, A. Eviatar, M. L. Kaiser, W. S. Kurth, A. J. Lazarus, K. W. Ogilvie, B. M. Pedersen, G. L. Siscoe and E. C. Sittler. The research was supported by grants from NASA Headquarters, JPL, the Office of Naval Research and the Bundesministerium, Forschung, Technologie, F. R. Germany.